

# Electrical Monitoring of $sp^3$ Defect Formation in Individual Carbon Nanotubes

Heather Wilson,<sup>†</sup> Sophie Ripp,<sup>‡</sup> Landon Prisbrey,<sup>†</sup> Morgan A. Brown,<sup>†</sup> Tal Sharf,<sup>†</sup> Daniel J. T. Myles,<sup>§</sup> Kerstin G. Blank,<sup>‡</sup> and Ethan D. Minot<sup>\*,†</sup>

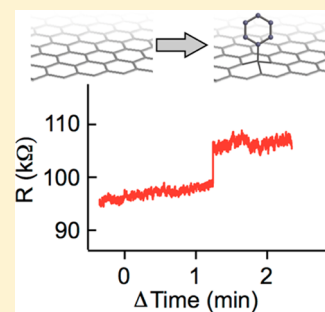
<sup>†</sup>Department of Physics, Oregon State University, Corvallis, Oregon 97331, United States

<sup>‡</sup>Institute for Molecules and Materials, Radboud University, Nijmegen, The Netherlands

<sup>§</sup>Department of Chemistry, Oregon State University, Corvallis, Oregon 97331, United States

## S Supporting Information

**ABSTRACT:** Many carbon nanotube (CNT) applications require precisely controlled chemical functionalization that is minimally disruptive to electrical performance. A promising approach is the generation of  $sp^3$  hybridized carbon atoms in the  $sp^2$ -bonded lattice. We have investigated the possibility of using a carboxylic acid-functionalized diazonium reagent to introduce a defined number of  $sp^3$  defects into electrically contacted CNTs. Having performed real-time measurements on individually contacted CNTs, we show that the formation of an individual defect is accompanied by an upward jump in resistance of approximately 6 k $\Omega$ . Additionally, we observe downward jumps in resistance of the same size, indicating that some defects are unstable. Our results are explained by a two-step reaction mechanism. Isolated aryl groups, formed in the first step, are unstable and dissociate on the minute time scale. Stable defect generation requires a second step: the coupling of a second aryl group adjacent to the first. Additional mechanistic understanding is provided by a systematic investigation of the gate voltage dependence of the reaction, showing that defect formation can be turned on and off. In summary, we demonstrate an unprecedented level of control over  $sp^3$  defect formation in electrically contacted CNTs, and prove that  $sp^3$  defects are minimally disruptive to the electrical performance of CNTs.



## INTRODUCTION

The functionalization of carbon nanotubes (CNTs) using diazonium salts shows great promise for a variety of applications. This covalent functionalization approach utilizes the high reactivity of diazonium radicals toward the  $sp^2$  lattice of the CNT, yielding an  $sp^3$  hybridized reaction product. The diazonium reaction has been used for dispersing CNTs in liquids,<sup>1,2</sup> sorting CNTs by chirality,<sup>3</sup> integrating CNTs into high-strength materials,<sup>4</sup> attaching CNTs to specific locations on a semiconductor device,<sup>5</sup> increasing the quantum yield of CNT photoluminescence,<sup>6</sup> and making CNT-based bioelectronic devices with biologically functional coatings.<sup>7–9</sup> Future applications include the attachment of single enzymes onto CNT sensors to study single-enzyme kinetics,<sup>10</sup> or the creation of optically active defect sites that can generate single photons on demand.<sup>11</sup>

In many of these applications, the number of covalently attached groups on a CNT needs to be precisely controlled. The ultimate level of control is the placement of a single functional group. This type of point functionalization has previously been achieved using oxidative chemistry on CNTs.<sup>12,13</sup> The generation of these oxidative defects involves the removal of at least one carbon atom, and the binding of one or more oxygen atoms directly to the CNT lattice. The introduction of an oxidative defect leads to a step-like change in

electrical resistance. For example, Goldsmith et al. report step sizes on the order of 300 k $\Omega$ .<sup>12</sup>

In contrast to oxidative defect generation, no carbon atoms are removed upon formation of an  $sp^3$  defect. Instead, one carbon atom converts from  $sp^2$  to  $sp^3$  hybridization. Theory predicts that an isolated  $sp^3$  defect in the CNT lattice causes a resistance change of approximately 6 k $\Omega$ ,<sup>14</sup> much less than the resistance change associated with an oxidative point defect. Since many applications of functionalized CNTs require preservation of electrical performance, a small change in resistance, such as that potentially introduced by the diazonium reaction, is advantageous. Additionally, the diazonium reagent can be functionalized with a variety of substituents so that many different chemical functionalities can be coupled onto the CNT surface.

The experimental observation of electron transport past a single  $sp^3$  defect has remained an outstanding challenge for over a decade. Despite exciting results with optical detection of single diazonium-generated defects in highly luminescent CNTs suspended in an agarose gel,<sup>15</sup> electrical detection of a single  $sp^3$  defect has not been achieved. Moreover, the

Received: November 17, 2015

Revised: January 1, 2016

possibility of simultaneously monitoring and controlling the generation of  $sp^3$  defects in CNTs has not been explored.

In this work, we use a carboxylic acid-functionalized diazonium reagent to introduce  $sp^3$  defects into electrically contacted CNTs. We quantify the change in electrical resistance associated with the creation of the resulting  $sp^3$  defects, including measurements with single defect resolution. We explore the stability of the generated  $sp^3$  defects and control the rate of defect formation. By monitoring the resistance of individual CNTs and simultaneously controlling the electrochemical potential, we demonstrate the possibility of preparing a CNT with a controlled degree of functionalization.

## RESULTS AND DISCUSSION

The reaction steps associated with diazonium functionalization are shown in Figure 1.<sup>16–20</sup> First, an aryl radical is formed and

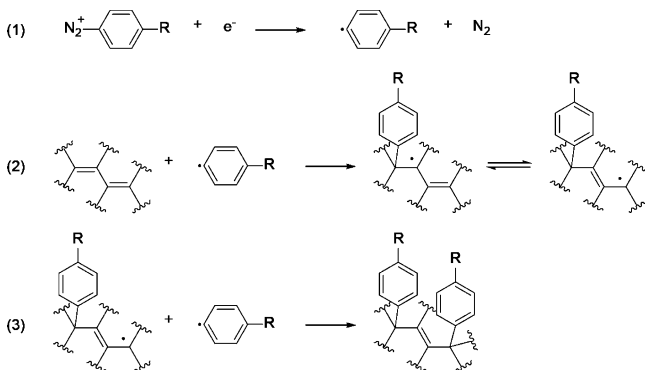


**Figure 1.** Mechanism of the diazonium reaction at low pH. (1) The diazonium cation is reduced by an electron originating from the CNT. The generation of the aryl radical is accompanied by the release of nitrogen gas. (2) The aryl radical reacts with an  $sp^2$  hybridized carbon atom of the CNT to form an  $sp^3$  hybridized covalent bond, leaving a radical on the CNT. (3) The presence of the radical in the vicinity of the attached phenyl ring promotes the attachment of a second diazonium radical to the CNT, stabilizing the structure.

$N_2$  is released. Second, the radical reacts with the CNT, creating an  $sp^3$ -hybridized carbon atom that protrudes from the cylindrical surface of the CNT. The first step, reduction of the diazonium cations into aryl radicals, can proceed via two possible mechanisms.<sup>19,20</sup> In one pathway, the diazonium cation first adsorbs on the CNT and is then reduced by an electron originating from the CNT. Previous authors have utilized an electrochemical driving potential between the CNT and the liquid to enhance this pathway.<sup>16</sup> In the other pathway, the diazonium cation is converted into the aryl radical following a reaction with  $OH^-$  ions in solution. In our experiments, we suppress the  $OH^-$  pathway by using a low pH buffer solution.<sup>19,20</sup> With the  $OH^-$  pathway suppressed, we are able to turn the reaction on and off by an electrochemical driving potential. For our work, we have chosen 4-carboxybenzene diazonium (CBD;  $R = COOH$ ) as the substituent.  $COOH$  is a versatile functional group that will easily allow further functionalization of the CNT for a number of applications.

Using the  $COOH$ -functionalized diazonium reagent CBD, we first investigated the electrical characteristics of a quasi-metallic CNT that has undergone varying degrees of functionalization by the diazonium reaction. Measuring a CNT with tens to hundreds of defects, we establish a framework for interpreting experiments that are designed to

observe the introduction of single defects. To quantify the electrical characteristics of CBD-functionalized CNTs, we determined the gate-dependent resistance of the CNT after multiple rounds of exposure to the reagent. The resistance was measured by applying a source-drain bias,  $V_{sd} = 25$  mV, and recording the source-drain current (see inset of Figure 2a). The

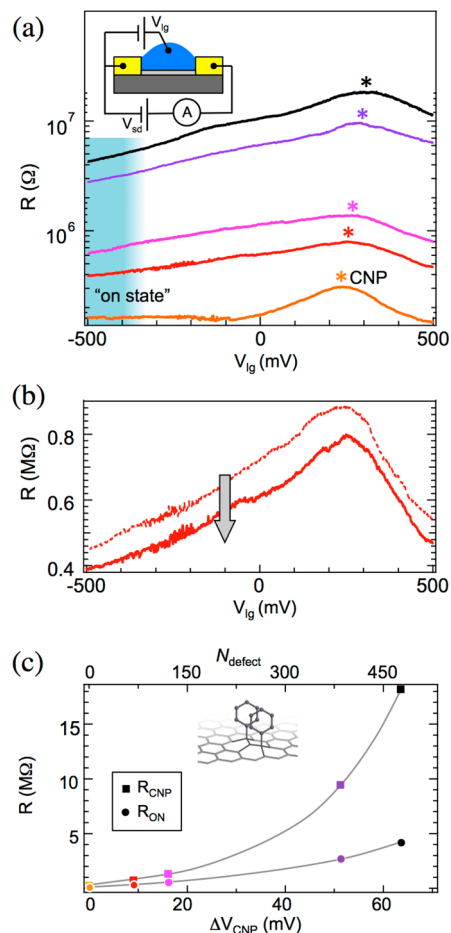


**Figure 2.** Electrical characteristics of a CNT exposed to the diazonium reagent. The CNT channel length was  $6 \mu\text{m}$ . (a) The resistance of a CNT before (orange) and after (red, pink, purple, black) four exposures to CBD. The gate voltage,  $V_{lg}$  (applied with a  $Ag/AgCl$  electrode), was used to tune the number of charge carriers in the CNT. The charge neutrality point coincides with the resistance peaks and is marked with an asterisk. The inset shows the circuit diagram used for measuring CNT resistance. (b) The resistance of the CNT after the first exposure to CBD. The dashed line was measured after washing the CNT for 2 min. The solid line was measured after washing the CNT for 10 min. (c) The on-state resistance  $R_{ON}$  and the charge neutrality point resistance,  $R_{CNP}$ , plotted as a function of the shift in charge neutrality point. The data points correspond to the five curves in Figure 2a. Gray lines are guides to the eye. The upper horizontal axis shows an estimate of the number of defects on the CNT (see main text).

liquid gate voltage,  $V_{lg}$ , was used to tune the number of charge carriers in the CNT from several thousand holes to several thousand electrons. In general, the resistance of a CNT is largest at the charge neutrality point (CNP), where the number of electron/holes is minimized. Both the position of the CNP and the magnitude of the CNT resistance are important parameters for characterizing the CNT electronic properties.

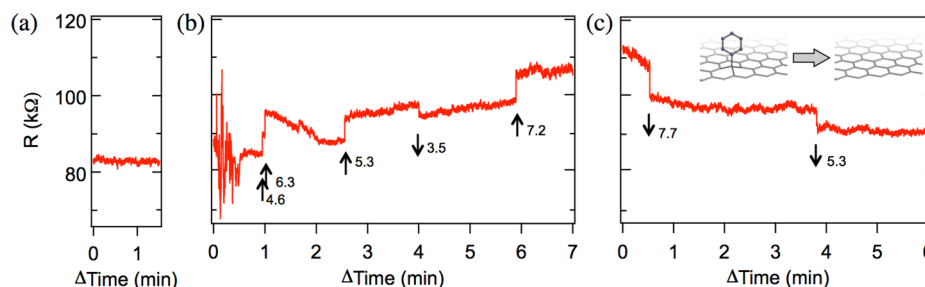


**Figure 3.** CNT resistance as a function of time recorded before, during, and after exposure to CBD. (a) Prior to CBD exposure (20 mM MES pH 4.6), a stable resistance was observed. (b) Upon exposure to 0.3 mM CBD solution (holding  $V_{\text{lg}}$  at 0 V using a gold electrode), several step-like changes in resistance were detected. (c) Washing the CNT in buffer shows only downward steps.  $R(t)$  data is collected at a rate of 500 samples per second. The size of each step (in  $\text{k}\Omega$ ) is indicated by arrows.

The low-resistance curve in Figure 2a shows the device characteristics before exposure to CBD. Microfluidics were then used to introduce a 1 mM solution of CBD. After 2 min of CBD exposure with  $V_{\text{lg}}$  held at  $-200$  mV with respect to the Ag/AgCl electrode, the resistance approximately doubled. The CNT was then washed in buffer for 2 min to ensure the reaction was stopped and the device was stable. The resistance was then measured (red dashed curve in Figure 2b), washed again for 10 min, and measured again (red solid curve in Figure 2a and 2b). This process was repeated three more times using increasingly aggressive exposure times and  $V_{\text{lg}}$  values. After each exposure to CBD, the resistance increased, and the CNP moved to the right. This observation invites a simple interpretation: upon exposure to CBD, aryl attachment occurs and  $\text{sp}^3$  defects are created in the CNT lattice. Each defect adds to the resistance of the CNT and causes chemical doping that leads to a shift in the CNP. We now build upon this basic interpretation.

The resistance curves obtained after washing the CBD-exposed CNT for 2 min differed from resistance curves measured after 10 min of washing (Figure 2b). A partial recovery of CNT conductivity was observed when extending the washing time. The recovery of CNT conductance suggests that some diazonium-generated defects are not permanent. Figure 1 depicts two types of  $\text{sp}^3$  defects: the isolated aryl group generated in the second reaction step and the aryl pair that is formed in the final step. Theoretical work predicts that an isolated aryl group attached to a CNT has a dissociation rate constant,  $k_{\text{off}}$ , on the order of minutes.<sup>21</sup> The recovery of CNT conductance that we observe in our experiment is therefore consistent with the dissociation of isolated aryl groups. In contrast, aryl pairs are predicted to be significantly more stable than isolated aryl groups.<sup>14,22</sup> Recent scanning tunneling microscope imaging of covalently bound aryl groups on graphite also supports the idea of stable aryl pair formation.<sup>23</sup> Therefore, we hypothesize that the recovery of CNT conductance is caused by the dissociation of isolated aryl groups, leaving behind a CNT functionalized with stable aryl pairs.

The dissociation of isolated aryl groups may not be the only explanation for the recovery of CNT conductance. The first step of the diazonium reaction involves the adsorption of diazonium cations on the CNT lattice. This may lead to doping and a concurrent change in CNT conductance. Unreacted diazonium cations adsorbed on the sidewall of the CNT may then be removed during the washing step so that the conductance can (partially) recover to its original value. However, previous work on graphene suggests that non-

covalently bound cations shift the CNP position ( $V_{\text{CNP}}$ ) without affecting  $R_{\text{CNP}}$  (a coating of charged molecules can change the number of charge carriers in a nanomaterial without changing carrier mobility).<sup>24</sup> Our data show a clear change in  $R_{\text{CNP}}$ , consequently, the desorption of unreacted cations is not a likely explanation for the recovery of CNT conductance.

We gain additional insight by investigating the relationship between  $R_{\text{CNP}}$  and the position of the charge neutrality point. For each  $R(V_{\text{lg}})$  curve in Figure 2a, we note  $R_{\text{CNP}}$  as well as the on-state resistance ( $R_{\text{ON}}$ ). The on-state resistance is measured at  $V_{\text{lg}} = -500$  mV, where the CNT is heavily doped with charge carriers.  $R_{\text{CNP}}$  and  $R_{\text{ON}}$  are then plotted against the shift in the charge neutrality point,  $\Delta V_{\text{CNP}}$  (see Figure 2c). Fitting a straight line to the first three  $R_{\text{CNP}}$  values yields a slope of  $64 \pm 4$   $\text{k}\Omega/\text{mV}$ . Fitting a straight line to the first three  $R_{\text{ON}}$  values yields a slope of  $29 \pm 3$   $\text{k}\Omega/\text{mV}$ . For larger  $\Delta V_{\text{CNP}}$ , the increase in resistance is superlinear.

We interpret the shift in  $V_{\text{CNP}}$  as a chemical doping effect. When an  $\text{sp}^2$  bonded carbon atom converts to the  $\text{sp}^3$  configuration, a delocalized electron is removed from the conduction band of the CNT. (The same effect occurs in graphene<sup>25</sup>). Additionally, the electron-withdrawing character of the COOH-group may contribute to chemical doping, and deprotonated carboxyl groups ( $\text{COO}^-$ ) may affect the charge neutrality point by electrostatic doping. These additional effects, however, can be considered small compared to the removal of one electron from the conduction band by  $\text{sp}^2$ -to- $\text{sp}^3$  conversion. We use the  $\text{sp}^2$ -to- $\text{sp}^3$  doping effect to estimate the number of defects in the CNT,  $N_{\text{defect}}$ . We first consider how chemical doping will impact  $V_{\text{CNP}}$ . The capacitance between an electrolyte gate and a metallic CNT is approximately  $0.4$   $\text{fF}/\mu\text{m}$  (equal to the quantum capacitance of a metallic CNT).<sup>26</sup> Therefore, the charge on the  $6$ - $\mu\text{m}$ -long CNT changes by  $15e$  when  $V_{\text{lg}}$  changes by  $1$  mV ( $e$  is the elementary charge). If chemical doping removes  $15$  electrons from the CNT, we expect  $\Delta V_{\text{CNP}} = +1$  mV, i.e., after chemical doping, a more positive liquid gate potential must be applied to reach the charge neutrality point. A stable defect (aryl pair) is depicted in Figure 2c. Each aryl pair is expected to remove  $2$  electrons from the CNT, thereby shifting  $V_{\text{CNP}}$  by  $0.13$  mV. The total number of defects in the CNT is then given by  $N_{\text{defect}} = \Delta V_{\text{CNP}}/[0.13$  mV]; see the upper horizontal axis of Figure 2c.

For small values of  $\Delta V_{\text{CNP}}$ , we interpret  $dR/dN_{\text{defect}}$  as the resistance per aryl pair. At small  $\Delta V_{\text{CNP}}$ , the density of aryl pairs is low so that we can assume that each pair acts as an independent resistor in series (the phase coherence length of electrons in CNTs is a few hundred nanometers<sup>27</sup>). We find  $dR_{\text{CNP}}/dN_{\text{defect}} = 8.5$   $\text{k}\Omega$ , while  $dR_{\text{ON}}/dN_{\text{defect}} = 3.9$   $\text{k}\Omega$ ,

suggesting that the resistance per aryl pair is gate-voltage dependent. Gate-dependent defect resistance has previously been observed for oxidative defects,<sup>13</sup> and has been predicted for  $sp^3$  defects.<sup>14</sup>

At larger values of  $\Delta V_{\text{CNP}}$ , Figure 2c shows a superlinear increase in  $R_{\text{ON}}$  and  $R_{\text{CNP}}$  with respect to  $\Delta V_{\text{CNP}}$ . At these higher defect densities, phase coherent scattering is known to cause localization effects.<sup>27</sup> In this regime, the overall resistance of the system is expected to be larger than the sum of individual resistors. The transition from linear to superlinear, seen in Figure 2c, is consistent with the crossover from low defect density to high defect density.

To test our understanding of  $sp^3$  defect generation by the diazonium reaction, we have subsequently performed real-time measurements of resistance versus time as a quasi-metallic CNT was exposed to CBD and then washed with buffer. Before the addition of CBD, the CNT resistance was stable at a value of  $R(t) = 82 \text{ k}\Omega$  with a standard deviation of less than  $1 \text{ k}\Omega$  (Figure 3a). No significant drift or any sudden steps in resistance were observed. Figure 3b shows  $R(t)$  after a droplet of CBD solution was added to the buffer solution. After the fluid settled, a slow and smooth variation in resistance was observed that was interrupted by abrupt steps. The size of each step, in units of  $\text{k}\Omega$ , is labeled in the Figure. The rise time of each step is faster than the time resolution of our measurement ( $2 \text{ ms}$ ). After replacing CBD with clean buffer solution, two downward steps were detected before  $R(t)$  settled at  $\sim 90 \text{ k}\Omega$ .

We interpret the upward and downward steps as the covalent bonding and unbonding of aryl groups to the CNT. The average step size is  $5.7 \text{ k}\Omega$ , in good agreement with theoretical studies predicting that the resistance of a short segment of metallic CNT changes from  $h/4e^2$  to approximately  $h/2e^2$  when one defect is added.<sup>14</sup> The frequency of downward steps is consistent with a dissociation rate on the minute time scale. This is the first direct observation of the resistance change caused by a single  $sp^3$  defect in a CNT.

It is interesting that the resistance change we have calculated for an aryl pair based on the data in Figure 2 ( $3.9\text{--}8.5 \text{ k}\Omega$ , depending on  $V_{\text{lg}}$ ) is similar to the resistance we have measured in our real-time recording where we most likely observe the attachment and detachment of isolated aryl groups ( $6 \pm 1 \text{ k}\Omega$ ). Lee et al. have considered both isolated aryl groups and aryl pairs in first-principle electron transport calculations. Their results predict that an aryl pair has a similar impact on CNT resistance as an isolated aryl group. We are consequently not able to directly distinguish these two types of defects based on the step size observed in our measurements.<sup>14</sup> A notable difference predicted to exist between the resistance changes of isolated aryl groups versus pairs is their different gate-dependence. Unfortunately, experiments probing such gate dependence are extremely challenging due to the instability of isolated aryl groups on the CNT.

The slow drift in resistance seen in Figure 3b,c is not fully understood. It may be explained by the adsorption (increase in Figure 3b) and desorption (decrease in Figure 3c) of unreacted diazonium cations, as discussed earlier. Alternatively, transient effects associated with fluid exchange may affect the CNT resistance. For example, the ratio of oxidized to reduced CBD molecules may alter the electrostatic potential of the solution as predicted by the Nernst equation.<sup>28</sup> Such changes in the solution potential would cause electrostatic gating and consequently influence the CNT resistance.

Control experiments such as shown in Figure 3a are an important aspect of our real-time measurements. We measured a number of other liquid-gated CNTs that exhibited less ideal  $R(t)$ . In some cases, the temporal fluctuations in resistance were too large ( $>1 \text{ k}\Omega$ ), and discrete steps were not discernible. In other cases, the devices exhibited random telegraph signals (RTS) that were unrelated to the introduction of CBD. Experiments by Sharf et al. have shown that RTS is caused by the fluctuating occupancy of trap states in the underlying oxide.<sup>29</sup> Therefore, we pursued additional measurements of  $R(t)$  using fully suspended CNTs (the CNT is surrounded by liquid and does not touch  $\text{SiO}_2$ ). These devices have minimal fluctuations in  $R$  and do not exhibit RTS.<sup>29</sup> A sequence of  $6 \text{ k}\Omega$  steps was replicated by exposing a suspended CNT device to CDB (see Supporting Information).

For the experiments depicted in Figures 2 and 3, the reaction was controlled by liquid exchange. An alternative method of controlling the reaction is to use  $V_{\text{lg}}$ . The electrochemical potential can be changed instantaneously, while liquid exchange requires a minimum equilibration time defined, for example, by the dead volume of the microfluidic system. Altering  $V_{\text{lg}}$  is therefore a promising pathway to achieve deterministic control of the reaction between CNTs and diazonium reagents.

According to the mechanism in Figure 1, the rate of radical formation is determined by electron transfer between the CNT and diazonium cations in solution. It is therefore likely that  $V_{\text{lg}}$  will have a direct influence on this process. Figure 4 shows a

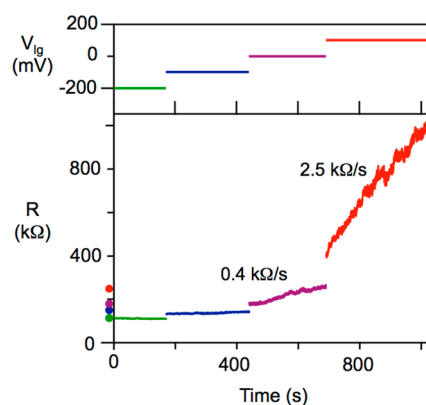


**Figure 4.** Resistance as a function of time while exposing a CNT to  $1 \text{ mM}$  CBD. A gold electrode was used to apply various liquid-gate voltages,  $V_{\text{lg}}$ . The upper panel shows the sequence of  $V_{\text{lg}}$  values:  $-200 \text{ mV}$  (green),  $-100 \text{ mV}$  (blue),  $0$  (purple) and  $+100 \text{ mV}$  (red). The four dots at  $t < 0$  show the resistance measured pre-exposure. The four dots at  $t > 1000$  show the resistance post-exposure.

series of measurements taken at various values of  $V_{\text{lg}}$ . First (before introducing CBD), the device resistance was measured at four values of  $V_{\text{lg}}$  ( $V_{\text{lg}} = -200 \text{ mV}$ ,  $-100 \text{ mV}$ ,  $0 \text{ mV}$ , and  $+100 \text{ mV}$ ; colored circles at  $t < 0$  in Figure 4). The increase in resistance as a function of  $V_{\text{lg}}$  is due to electrostatic doping. After introducing CBD,  $V_{\text{lg}}$  was held constant at  $-200 \text{ mV}$  for approximately  $200 \text{ s}$ . The device resistance did not change, indicating that the reaction did not proceed. Next,  $V_{\text{lg}}$  was held at  $-100 \text{ mV}$  for approximately  $200 \text{ s}$ , leading to a slow increase in  $R$ . The gate voltage was increased further two more times. When  $V_{\text{lg}}$  was held at  $+100 \text{ mV}$ ,  $dR/dt = 2.5 \text{ k}\Omega/\text{s}$ . The experiment was concluded by measuring device resistance at the four values of  $V_{\text{lg}}$  (Figure 4, colored circles at  $t > 1000$ ).

From Figure 4, we conclude that the reaction between CBD and the CNT is stalled when  $V_{\text{lg}} = -200$  mV, but proceeds rapidly at  $V_{\text{lg}} = +100$  mV. This voltage-controlled reaction rate is consistent with the reaction mechanism shown in Figure 1, highlighting the importance of electrochemical aryl radical formation for initiating the reaction. The required electron transfer between the CNT and the diazonium cation does not proceed if  $V_{\text{lg}}$  is too negative. We note that the value of  $V_{\text{lg}}$  required to reach a specific rate  $dR/dt$  varied between different CNT devices. Sources of reaction rate variability include the electrode used to apply  $V_{\text{lg}}$  (i.e., the interface potential at the metal-liquid interface), and the age of the diazonium solution. Most likely also the CNT diameter affects the reaction rate.

Figure 4 clearly demonstrates that the diazonium reaction can be turned on using  $V_{\text{lg}}$ . In a second experiment (see SI), we have further shown that the gate voltage can turn off the reaction equally well. This opens the door for the controlled functionalization of a CNT with single  $\text{sp}^3$  defect resolution. For example, the following protocol could be employed. (1) Single defects can be created when holding  $V_{\text{lg}}$  at 0 mV until an upward step in resistance is observed. (2) The stability of this nascent defect can be tested by switching  $V_{\text{lg}}$  to  $-200$  mV and holding the device at this value for several minutes. Devices that contain an unstable isolated aryl defect will exhibit a downward step in resistance. If a downward step is observed, steps 1 and 2 can be repeated until a stable defect pair is obtained. (3) If a stable defect is suspected, the reagent can be removed. After extensively washing the device in buffer,  $R(V_{\text{lg}})$  should be measured to confirm the defect configuration. Such a protocol would be ideally suited for future applications such as attaching single enzymes onto CNT sensors where a single reactive group on the CNT is desired.<sup>10</sup> Alternatively, the protocol may be employed for creating optically active single defects that generate single photons on-demand.<sup>11</sup>

In conclusion, we have used electrical measurements to monitor the attachment of a single diazonium-generated  $\text{sp}^3$  defect in real time. As a direct consequence of our single defect resolution, we have quantified the associated resistance change of approximately 6 k $\Omega$ . (In comparison, oxidative point defects add significantly more resistance.<sup>12</sup>) The exact value of this resistance change may be determined by several factors such as the diameter, the chirality, and the doping level of the CNT, as well as the nature of the substituent on the diazonium reactant. A more detailed investigation of these factors is an interesting direction for future research. Our measurements of defect healing support theoretical predictions that isolated aryl groups easily dissociate from the CNT lattice and that only aryl pairs form stable defects. Having combined real-time measurements with real-time control of the diazonium reaction, we show that the reaction can be turned on and off using the gate voltage as a control parameter. Overall, these results provide the basis for developing a well-defined procedure capable of controlling the number of stable aryl groups on an electrically contacted CNT. Moreover, as a variety of substituents can be grafted onto diazonium reagents, this approach offers a flexible, new route to the chemical functionalization of CNTs with minimal impact on resistance.

## MATERIAL AND METHODS

Carbon nanotube field-effect transistors (CNT-FETs) were fabricated using standard photolithographic and metal deposition techniques. CNTs were grown from catalyst islands (1 nm Ti, 40 nm  $\text{SiO}_2$ , 1 nm Fe) on a Si/ $\text{SiO}_2$  substrate by chemical

vapor deposition (CVD). Metal electrodes were evaporated on top (30 nm Au with 2 nm Cr sticking layer). We have observed equivalent results by growing CNTs after electrode deposition. When growing CNTs in the last step, we fabricated metal electrodes (1 nm Ti, 50 nm Pt), deposited catalyst islands on top of the electrodes, then grew CNTs by CVD. An  $\text{SiO}_2$  passivation layer (80 nm thickness) was deposited on top of the electrodes to reduce Faradaic currents between the metal and the liquid environment. The distance between source and drain electrodes was 4  $\mu\text{m}$ , and the CNT channel length was  $\geq 4$   $\mu\text{m}$ . After fabrication, we selected devices with a single CNT connecting the source and drain electrodes. CNT channel lengths and diameters were measured by atomic force microscopy. Diameters ranged from 1.5–3 nm.

4-Carboxybenzene diazonium (CBD) was synthesized using a previously established protocol.<sup>30</sup> Buffer solution (20 mM MES pH 4.6) and CBD solution in buffer were applied to the CNT devices either by placing a drop on the chip by hand, or by flowing solution through a microfluidic channel. A CBD concentration between 300  $\mu\text{M}$  and 1 mM was chosen to allow for real-time observations. When applying solution by hand, a few hundred microliters was placed on the surface of the chip using a pipet tip. To stop the solution from spreading, a Parafilm dam was melted onto the chip with gentle heat (hot plate at 115  $^\circ\text{C}$  for 2 min) prior to wetting the chip. When using microfluidics, a PDMS flow channel was pressed on the surface of the chip. Flow was achieved by pressurizing the head of the fluid reservoir with nitrogen gas (approximately 5 psi). A microfluidic selector valve (Idex) was used to exchange buffer solution with CBD solution.

Electrical measurements were obtained in a semiconductor probe station. A Yokogawa GS200 DC Voltage/Current Source was used to supply the gating potential,  $V_{\text{lg}}$ . When liquid was delivered by microfluidics,  $V_{\text{lg}}$  was applied using a Ag/AgCl reference electrode. When liquid was applied by hand, an on-chip electrode (Au or Pt) was used to apply  $V_{\text{lg}}$ . A Stanford Research Systems Low-Noise Current Preamplifier SR570 was used to measure source-drain current and supply the source-drain bias of 25 mV. The liquid-gate potential was limited to a range in which Faradaic currents were less than 500 pA.

## ASSOCIATED CONTENT

### Supporting Information

The Supporting Information is available free of charge on the ACS Publications website at DOI: 10.1021/acs.jpcc.5b11272.

Experiment using a fully suspended CNT (the CNT does not contact an insulating substrate) demonstrating electrical detection of single defects and experiment demonstrating the voltage-controlled start/stop of the diazonium reaction (PDF)

## AUTHOR INFORMATION

### Corresponding Author

\*E-mail: ethan.minot@oregonstate.edu.

### Author Contributions

The manuscript was written through contributions of all authors. All authors have given approval to the final version of the manuscript.

### Notes

The authors declare no competing financial interest.

## ACKNOWLEDGMENTS

This work was financially supported by the Human Frontier Science Program (HFSP; Grant RGY0058/2010). H.W. acknowledges support from an Undergraduate Research, Innovation, Scholarship and Creativity (URISC) grant. Sample fabrication was performed at the MaSC Facility at Oregon State University and the Cornell node of the National Nanofabrication Infrastructure Network, which is supported by the National Science Foundation (ECCS-15420819). We thank Dr. Richard Martel for valuable discussions. We thank Matthew Glaus for assistance with the preparation of the diazonium salt.

## REFERENCES

- (1) Chen, J.; Rao, A. M.; Lyuksyutov, S.; Itkis, M. E.; Hamon, M. A.; Hu, H.; Cohn, R. W.; Eklund, P. C.; Colbert, D. T.; Smalley, R. E.; et al. Dissolution of Full-Length Single-Walled Carbon Nanotubes. *J. Phys. Chem. B* **2001**, *105*, 2525–2528.
- (2) Amiri, A.; Zardini, H. Z.; Shanbedi, M.; Maghrebi, M.; Baniadam, M.; Tolueinia, B. Efficient Method for Functionalization of Carbon Nanotubes by Lysine and Improved Antimicrobial Activity and Water-Dispersion. *Mater. Lett.* **2012**, *72*, 153–156.
- (3) Strano, M. S.; Dyke, C. A.; Usrey, M. L.; Barone, P. W.; Allen, M. J.; Shan, H.; Kittrell, C.; Hauge, R. H.; Tour, J. M.; Smalley, R. E. Electronic Structure Control of Single-Walled Carbon Nanotube Functionalization. *Science* **2003**, *301*, 1519–1522.
- (4) Mitchell, C. A.; Bahr, J. L.; Arepalli, S.; Tour, J. M.; Krishnamoorti, R. Dispersion of Functionalized Carbon Nanotubes in Polystyrene. *Macromolecules* **2002**, *35*, 8825–8830.
- (5) Klinke, C.; Hannon, J. B.; Afzali, A.; Avouris, P. Field-Effect Transistors Assembled from Functionalized Carbon Nanotubes. *Nano Lett.* **2006**, *6*, 906–910.
- (6) Piao, Y.; Meany, B.; Powell, L. R.; Valley, N.; Kwon, H.; Schatz, G. C.; Wang, Y. Brightening of Carbon Nanotube Photoluminescence through the Incorporation of sp<sup>3</sup> Defects. *Nat. Chem.* **2013**, *5*, 840–845.
- (7) Baker, S. E.; Tse, K.-Y.; Hindin, E.; Nichols, B. M.; Lasseter Clare, T.; Hamers, R. J. Covalent Functionalization for Biomolecular Recognition on Vertically Aligned Carbon Nanofibers. *Chem. Mater.* **2005**, *17*, 4971–4978.
- (8) Graff, R. A.; Swanson, T. M.; Strano, M. S. Synthesis of Nickel–Nitrilotriacetic Acid Coupled Single-Walled Carbon Nanotubes for Directed Self-Assembly with Polyhistidine-Tagged Proteins. *Chem. Mater.* **2008**, *20*, 1824–1829.
- (9) Goldsmith, B. R.; Mitala, J. J.; Josue, J.; Castro, A.; Lerner, M. B.; Bayburt, T. H.; Khamis, S. M.; Jones, R. A.; Brand, J. G.; Sligar, S. G.; et al. Biomimetic Chemical Sensors Using Nanoelectronic Readout of Olfactory Receptor Proteins. *ACS Nano* **2011**, *5*, 5408–5416.
- (10) Choi, Y.; Moody, I. S.; Sims, P. C.; Hunt, S. R.; Corso, B. L.; Perez, I.; Weiss, G. A.; Collins, P. G. Single-Molecule Lysozyme Dynamics Monitored by an Electronic Circuit. *Science* **2012**, *335*, 319–324.
- (11) Ma, X.; Hartmann, N. F.; Baldwin, J. K. S.; Doorn, S. K.; Htoon, H. Room-Temperature Single-Photon Generation from Solitary Dopants of Carbon Nanotubes. *Nat. Nanotechnol.* **2015**, *10*, 671.
- (12) Goldsmith, B. R.; Coroneus, J. G.; Khalap, V. R.; Kane, A. A.; Weiss, G. A.; Collins, P. G. Conductance-Controlled Point Functionalization of Single-Walled Carbon Nanotubes. *Science (Washington, DC, U. S.)* **2007**, *315*, 77–81.
- (13) Prisbrey, L.; Roundy, D.; Blank, K.; Fifield, L. S.; Minot, E. D. Electrical Characteristics of Carbon Nanotube Devices Prepared with Single Oxidative Point Defects. *J. Phys. Chem. C* **2012**, *116*, 1961–1965.
- (14) Lee, Y.-S.; Nardelli, M. B.; Marzari, N. Band Structure and Quantum Conductance of Nanostructures from Maximally Localized Wannier Functions: The Case of Functionalized Carbon Nanotubes. *Phys. Rev. Lett.* **2005**, *95*, 076804.
- (15) Cagnet, L.; Tsybouski, D. A.; Rocha, J.-D. R.; Doyle, C. D.; Tour, J. M.; Weisman, R. B. Stepwise Quenching of Exciton Fluorescence in Carbon Nanotubes by Single-Molecule Reactions. *Science* **2007**, *316*, 1465–1468.
- (16) Bahr, J. L.; Yang, J.; Kosynkin, D. V.; Bronikowski, M. J.; Smalley, R. E.; Tour, J. M. Functionalization of Carbon Nanotubes by Electrochemical Reduction of Aryl Diazonium Salts: A Bucky Paper Electrode. *J. Am. Chem. Soc.* **2001**, *123*, 6536–6542.
- (17) Usrey, M. L.; Lippmann, E. S.; Strano, M. S. Evidence for a Two-Step Mechanism in Electronically Selective Single-Walled Carbon Nanotube Reactions. *J. Am. Chem. Soc.* **2005**, *127*, 16129–16135.
- (18) Wang, H.; Xu, J. Theoretical Evidence for a Two-Step Mechanism in the Functionalization Single-Walled Carbon Nanotube by Aryl Diazonium Salts: Comparing Effect of Different Substituent Group. *Chem. Phys. Lett.* **2009**, *477*, 176–178.
- (19) Schmidt, G.; Gallon, S.; Esnouf, S.; Bourgoin, J.-P.; Chenevier, P. Mechanism of the Coupling of Diazonium to Single-Walled Carbon Nanotubes and Its Consequences. *Chem. - Eur. J.* **2009**, *15*, 2101–2110.
- (20) Dyke, C.; Stewart, M.; Maya, F.; Tour, J. Diazonium-Based Functionalization of Carbon Nanotubes: XPS and GC-MS Analysis and Mechanistic Implications. *Synlett* **2004**, 155.
- (21) Margine, E. R.; Bocquet, M.-L.; Blase, X. Thermal Stability of Graphene and Nanotube Covalent Functionalization. *Nano Lett.* **2008**, *8*, 3315–3319.
- (22) López-Bezanilla, A.; Triozon, F.; Latil, S.; Blase, X.; Roche, S. Effect of the Chemical Functionalization on Charge Transport in Carbon Nanotubes at the Mesoscopic Scale. *Nano Lett.* **2009**, *9*, 940–944.
- (23) Greenwood, J.; Phan, T. H.; Fujita, Y.; Li, Z.; Ivasenko, O.; Vanderlinden, W.; Van Gorp, H.; Fredericx, W.; Lu, G.; Tahara, K.; et al. Covalent Modification of Graphene and Graphite Using Diazonium Chemistry: Tunable Grafting and Nanomanipulation. *ACS Nano* **2015**, *9*, 5520–5535.
- (24) Farmer, D. B.; Golizadeh-Mojarad, R.; Perebeinos, V.; Lin, Y.-M.; Tulevski, G. S.; Tsang, J. C.; Avouris, P. Chemical Doping and Electron-Hole Conduction Asymmetry in Graphene Devices. *Nano Lett.* **2009**, *9*, 388–392.
- (25) Pembroke, E.; Ruan, G.; Sinitskii, A.; Corley, D. A.; Yan, Z.; Sun, Z.; Tour, J. M. Effect of Anchor and Functional Groups in Functionalized Graphene Devices. *Nano Res.* **2013**, *6*, 138–148.
- (26) Rosenblatt, S.; Yaish, Y.; Park, J.; Gore, J.; Sazonova, V.; McEuen, P. L. High Performance Electrolyte Gated Carbon Nanotube Transistors. *Nano Lett.* **2002**, *2*, 869–872.
- (27) Sundqvist, P.; Garcia-Vidal, F. J.; Flores, F.; Moreno-Moreno, M.; Gómez-Navarro, C.; Bunch, J. S.; Gómez-Herrero, J. Voltage and Length-Dependent Phase Diagram of the Electronic Transport in Carbon Nanotubes. *Nano Lett.* **2007**, *7*, 2568–2573.
- (28) Larrimore, L.; Nad, S.; Zhou, X.; Abruña, H.; McEuen, P. L. Probing Electrostatic Potentials in Solution with Carbon Nanotube Transistors. *Nano Lett.* **2006**, *6*, 1329–1333.
- (29) Sharf, T.; Wang, N.-P.; Kevek, J. W.; Brown, M. A.; Wilson, H.; Heinze, S.; Minot, E. D. Single Electron Charge Sensitivity of Liquid-Gated Carbon Nanotube Transistors. *Nano Lett.* **2014**, *14*, 4925–4930.
- (30) Hanson, P.; Jones, J. R.; Taylor, A. B.; Walton, P. H.; Timms, A. W. Sandmeyer Reactions. Part 7.1 An Investigation into the Reduction Steps of Sandmeyer Hydroxylation and Chlorination Reactions. *J. Chem. Soc. Perkin Trans. 2* **2002**, 1135–1150.